J. Braz. Chem. Soc., Vol. 24, No. 2, 1-11, 2013.
Printed in Brazil - ©2013 Sociedade Brasileira de Química
0103 - 5053 $6.00+0.00

Article

Effect of Iron Content on the Catalytic Properties of Activated Carbon-Supported Magnetite Derived from Biomass

Sirlene B. Lima,[a,b] Sarah Maria S. Borges,[a,b] Maria do Carmo Rangel*[*,a,b] and Sergio G. Marchetti[c]

[a]*Instituto de Química, Universidade Federal da Bahia, Campus Universitário de Ondina, Federação, 40290-170 Salvador-BA, Brazil*

[b]*Instituto de Ciência e Tecnologia de Materiais Complexos Funcionais. Instituto de Química (INOMAT), Universidade de Campinas (Unicamp), Bloco J, Rua Monteiro Lobato, Cidade Universitária Zeferino Vaz, 13083-970 Campinas-SP, Brazil*

[c]*Centro de Investigación y Desarrollo em Ciencias Aplicadas "Dr. Jorge J. Ronco" (CINDECA), Facultad de Ciencias Exactas, Universidad Nacional de La Plata, 1900, 47 y 115, La Plata, Argentina*

Nos últimos tempos, a intensa atividade humana levou a um aumento de resíduos agrícolas no meio ambiente. Visando a encontrar novas aplicações para estes materiais estudou-se, neste trabalho, o efeito do teor de ferro (2.5, 5, 10 e 15%) sobre as propriedades catalíticas de óxido de ferro suportado em carvão ativado, preparado a partir de cascas de coco. O teor de ferro afetou as propriedades texturais e redutoras dos sólidos. Detectou-se hematita na amostra mais pobre em ferro e magnetita com um núcleo de hematita nas demais. Estes catalisadores foram eficazes na remoção do azul de metileno em soluções aquosas por adsorção e pela reação de Fenton. O sólido com 15% de ferro foi o mais ativo, provavelmente devido à maior quantidade de sítios ativos na superfície. Estes catalisadores são ambientalmente amigáveis, contribuindo para a redução de resíduos sólidos no meio ambiente e purificação de efluentes têxteis, preservando os recursos hídricos.

In recent times, the intense human activity has led to an increase of the agriculture wastes in the environment. "In order to find new applications for these materials, the effect of iron content (2.5, 5, 10 and 15%) on the catalytic properties of activated carbon-supported iron oxide, prepared from coconut shells, was studied. The iron amount affected the textural and reducing properties of the solids and particle sizes. Hematite was found for the most iron-poor sample, while particles of magnetite with a core of hematite were found for the others. These catalysts were effective in the methylene blue removal from aqueous solutions by adsorption and Fenton reaction. The solid with 15% of iron was the most active one probably due to the highest iron amount on the surface. These catalysts are environmentally friendly, contributing to the decrease of the solid wastes in the environment as well as to purify textile effluents, preserving water resources.

Keywords: coconut shell, activated carbon, magnetite, dyes, methylene blue

Introduction

In recent times, the generation of waste materials from agriculture and their disposal in the environment has been one of the main concerns faced worldwide. Most of the time, these materials are disposed directly in the environment, causing an excessive accumulation of organic matter. Although this type of pollutant is biodegradable, a minimum time is required for its mineralization. In addition, because of the large human activity, there is an increasing difficulty for their natural recycling.[1] An attractive option to overcome this problem is to use the solid wastes as energy source or raw materials to obtain high value products, such as activated carbons. They can be prepared from various kinds of materials such as coconut shells, wood, lignin, oil, peat, coke, bones, seeds, sawdust, rice hulls, waste fertilizers and polymers.[2,3]

*e-mail: mcarmov@ufba.br

Activated carbons have attracted considerable attention in recent years due to their potential use for different applications, due to their physical and chemical properties, such as high hardness, thermal resistance, corrosion resistance and electrical conductivity, resistance to acids and bases, functional groups on the surface, ease of adsorbing ions and high specific surface area[4] Most of these properties can be controlled during the preparation of active carbons.[3] Because of these features, they have found applications in several fields such as in the adsorption of gases or liquids or in the recovery and purification of chemicals, as well as for the storage of hydrogen in fuel cells.[5,6] In addition, they have been used as catalysts and supports in various reactions like ethylbenzene dehydrogenation,[7,8] phenol removal from industrial effluents[9] and nitrate or organic dye removal from residual water.[10-13]

Among the organic dyes, the textile ones are known to have a high potential for polluting the water resources. When disposed of in the environment, the highly colored components, coming from their incomplete fixation on textile substrates, cause an undesirable color in water and can lead to significant disturbance in ecological systems. In addition, they may be harmful to human health since these compounds are highly carcinogenic.[14] Therefore, their degradation is necessary to ensure public health and safety. However, they have complex structures difficult to be decomposed, requiring the Advanced Oxidation Processes (AOPs). Among them, the Fenton reaction is one of the most promising processes for removing organic dyes, with the advantages of simplicity, efficiency and low cost investment, besides the mild reaction conditions.[15]

The Fenton process involves the reaction between Fe^{2+} species and hydrogen peroxide, generating hydroxyl radicals, a very strong oxidizing species that unselectively react with most of the contaminants in water.[16,17] In addition, the process uses an iron catalyst and hydrogen peroxide, which are less expensive and easier and safer to handle than the other oxidizing chemicals. In the presence of a heterogeneous catalyst (Fenton-like or modified Fenton reaction), the process works at circumneutral pH, avoiding the sludge formation and offering the possibility of recycling the catalyst, which are advantages over the traditional method.[18] However, the reaction is slower than in classical Fenton process and thus several studies have been carried out aiming to find efficient catalysts for the heterogeneous Fenton-like systems.[19] Among several iron compounds investigated, magnetite is recognized as the most efficient catalyst, besides being environmentally friendly, inexpensive and available in great reserves.[20] Also, it is magnetic and can be easily separated from the final solution by a magnet, making possible its application in flow-bed technologies.

Several works[20-22] have demonstrated that the iron oxide activity largely depends on its characteristics such as crystallinity, specific surface area and oxidation state. Therefore, the preparation method, the use of dopants and the kind of supports become important features to be considered in the development of new catalysts since they largely determine the final properties of the solids. The use of a support is especially convenient in order to avoid the nanoparticle aggregation, as found for porous silica[23] and zeolites.[24] In addition, the support can increase the adsorption capacity of iron oxide as observed for montmorillonite-supported magnetite.[25] The use of activated carbon-supported magnetite was also a successful attempt at combining the magnetic and adsorption properties of these materials, which have attracted increasing attention from researchers worldwide. Castro *et al.*,[13] for instance, have found that activated carbon-supported goethite was an efficient catalyst to remove methylene blue from aqueous solutions, by a combined process of adsorption and oxidation by hydrogen peroxide. Also, Oliveira *et al.*[26] have observed that activated carbon-supported maghemite efficiently removed drimaren red from aqueous solutions by adsorption. On the other hand, Pereira *et al*[27] have noted that an activated carbon-supported iron composite (Fe_3O_4-Fe^0) was able to remove drimaren red from aqueous solutions by the Fenton reaction.

Aiming to develop new systems for removing organic dyes from aqueous effluents, as well as to use agriculture wastes, the effect of iron content on the catalytic properties of activated carbon-supported magnetite derived from coconut shells was studied in this work. The catalysts were evaluated in the removal of methylene blue, used as a model compound of textile dyes.

Experimental

Catalysts preparation

Samples were prepared from coconut shells collected in Lauro de Freitas City, in the metropolitan region of Salvador City, Bahia State, Brazil. The biomass was exposed to the sun for removing moisture, avoiding fungi propagation. It was then rinsed with distilled water to remove dust and inorganic impurities, which can cause changes in the final material. After these steps, it was dried in an oven at 120 °C for 20 h and kept in a desiccator to cool down to room temperature. The coconut mesocarp was triturated in a mill and sieved to 100 mesh.

Activated carbons were prepared by chemical activation using magnesium chloride as activating agent. The coconut mesocarp (10 g) was mixed with the activating agent (5 g) (weight ratio of biomass to activating agent of 2), soaked with water and kept in a rotary evaporator (80 rpm) for 2 h. The material was then dried in an oven at 120 ºC, for 24 h. Next, the materials were placed in a quartz cell, heated (10 °C min^{-1}) under nitrogen flow up to 600 ºC and kept at this temperature for 2 h. After this step, the system was cooled down to room temperature under flowing nitrogen. The activated carbon produced was rinsed three times with a 3% hydrochloric acid solution and then with distilled water at 80 °C. The system was centrifuged to remove the residues of the activating agents. The steps of washing and centrifugation were repeated up to pH between 6 and 7. The activated carbons were dried at 120 °C, for 24 h.

The catalysts were obtained by the impregnation of the activated carbons with an aqueous solution of iron nitrate, with appropriate concentrations to achieve the iron contents of 2.5, 5, 10 and 15% in the final solids. The system was kept under stirring (80 rpm) for 2 h. The catalyst was dried at 120 °C, for 24 h and heated (10 °C min^{-1}) under nitrogen flow (100 mL min^{-1}) up to 450 °C, being kept at this temperature for 2 h.

Catalysts characterization

The samples were characterized by chemical analysis, Fourier transform infrared spectroscopy (FTIR), X-ray diffraction (XRD), Mössbauer spectroscopy, specific surface area and porosity measurements and temperature programmed reduction (TPR).

The chemical composition of the coconut mesocarp was determined by X-ray fluorescence spectrometry using a Shimadzu model XRF-700HS apparatus. The sample was mixed with boric acid, milled and pressed (3 tons for 5 min) to obtain discs. The Fourier transform infrared spectra were achieved on a FTIR Bomem MB100 instrument, in the range 4000 to 400 cm^{-1}, using discs of the sample diluted in potassium bromide. The X-ray diffraction profiles of the catalysts were obtained by the powder method on a Siemens D5005 equipment using Cu K_α radiation and a nickel filter. The phases in the samples were identified by comparing the X-ray patterns with the JCPDS-ICDD files. The particle sizes of magnetite were calculated by Scherrer equation using the (311) plane of magnetite.

Mössbauer spectra were obtained in a spectrometer equipped with twelve channels with constant acceleration and geometry of transmission. A source of ^{57}Co was used in a matrix of Rh of 50 me normal. All isomeric shifts were related to a standard at 25 ºC. For each component of the spectra, Lorentzian lines of the same width were used. All the spectra were fitted and were obtained the distributions of the hyperfine parameter to quantify the different phase of the iron oxides. The spectra were obtained at room temperature and folded to minimize geometric effects, being evaluated using a commercial computer fitting program named Recoil.

The specific surface area and porosity measurements were performed on a Micromeritics ASAP 2010 model equipment. The sample (0.3 g) was placed in a glass cell which was evacuated up to 10 μm Hg and heated (10 min^{-1}) under nitrogen flow (60 mL min^{-1}) up to 160 °C, being kept at this temperature for 30 min, to remove moisture and volatiles from the sample. Subsequently, the solid was submitted to a second cleaning step under vacuum of 1 μm Hg. Then, the cell was immersed in liquid nitrogen and the measurements were done. The desorption branch was used to calculate the pore size distribution of the macro and mesopores, through the Barret-Joyner-Halenda (BJH) mathematical model. The micropore and mesoporous volumes were calculated by the *t*-curve and the BJH method, respectively. The specific surface area was calculated by the Brunauer-Emmett-Teller model (BET) using the adsorption data in a range from 0.05 to 0.2 of relative pressure.

The curves of temperature programmed reduction (TPR) were recorded on a Micromeritics TPR/TPD 2900 model equipment. The sample (0.3 g) was placed in a quartz cell and submitted to a pre-treatment to remove impurities and moisture. The sample was then heated (10 °C min^{-1}) under nitrogen flow (60 mL min^{-1}) up to 160 °C and remained at this temperature for 30 min. The nitrogen flow was replaced by a gas mixture (5% H_2/N_2) and the sample was heated (10 °C min^{-1}) up to 1000 °C under the mixture flow (60 mL min^{-1}).

Catalysts evaluation

The catalysts were evaluated in the degradation of methylene blue, using the Fenton reaction. The reaction was performed using 2 mL of a 30% hydrogen peroxide solution, 10 mL of a solution of methylene blue (10 mg L^{-1}) in the presence of the catalyst (0.01 g) at room temperature, under stirring. Different reaction times were used: 5, 15, 30, 45, 60 and 90 min. After each time, the solution was isolated by filtration and analyzed on a Shimadzu model 2450 UV spectrometer, in the visible region, using a wavelength of 665 nm (characteristic of methylene blue). Other experiments in the absence of hydrogen peroxide were also carried out in the same conditions in order to evaluate the adsorption capacity of the solids.

Table 1. Chemical composition of the coconut shell (mesocarp)

Element	C	O	K	Cl	Si	Na	Ca	Mg	P	Al
Concentration / %	63.043	30.783	3.212	1.043	0.506	0.451	0.333	0.227	0.146	0.046

Results and Discussion

Chemical composition of the coconut shell

Table 1 shows the chemical composition of the coconut mesocarp. It can be noted that the sample has high carbon content, the major requirement in the choice of the raw material for preparing activated carbons. Small amounts of silicon, potassium, calcium, phosphorus, aluminum and other elements were also found.

Fourier transform infrared spectroscopy

The FTIR spectra of the catalysts were similar, as shown in Figure 1. They consist of few weak bands, indicating few types of oxygenated groups on the solid surface.[28] It can be noted a band at 3400 cm^{-1}, which can be attributed to the stretching vibrations of the OH bonds in both phenols and water.[29] For all spectra, a band between 1570 and 1580 cm^{-1} is detected, being ascribed to the stretching vibration of C=C bonds characteristic of aromatic groups.[30] The band observed at 1380 cm^{-1} is related to O-H deformation vibration and confirms the presence of OH groups in phenols.[31] The band around 595 cm^{-1} is attributed to the OH deformation vibration outside the plane.[32]

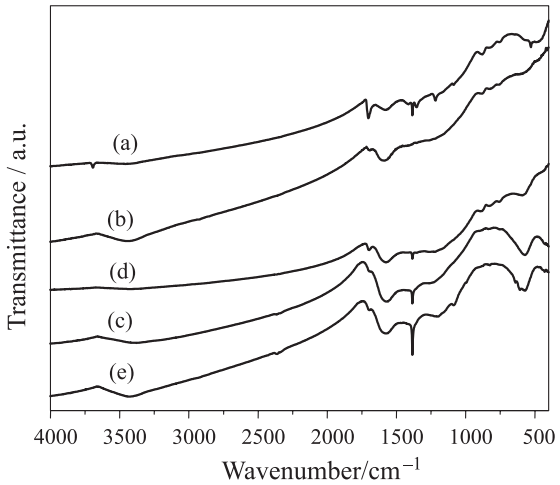

Figure 1. Infrared spectra for the (a) AC sample (activated carbon), and for the (b) 2.5IAC, (c) 5IAC, (d) 10IAC and (e) 15IAC samples (activated carbon-supported iron oxide). The numbers represent the iron amount (wt.%) in the solids.

X-ray diffration

Figure 2 shows the XRD patterns for the support and for the catalysts. The diffractogram of the support shows an amorphous halo at around 25°, which is typical of activated carbon.[33] It can be also noted peaks related to magnesium oxide, MgO (JCPDS card 77-2364) and magnesium carbide, Mg_2C_3 (JCPDS card 47-1556) coming from magnesium chloride used as activating agent. It is well known that magnesium carbides can be obtained by the reaction of magnesium and carbon to produce MgC_2 below 500 °C and Mg_2C_3 between 500 and 700 °C.[34] The production of magnesium carbide at 600 °C in the present work is also in agreement with previous work.[35] Therefore, the washing steps were not enough for removing the activating agent, leading to the production of magnesium-containing phases.

Except for the most iron-poor sample (2.5IAC), all XRD patterns of the catalysts indicated peaks related to both amorphous carbon[33] and magnetite (JCPDS card 88-0315). The 2.5IAC sample showed a typical profile

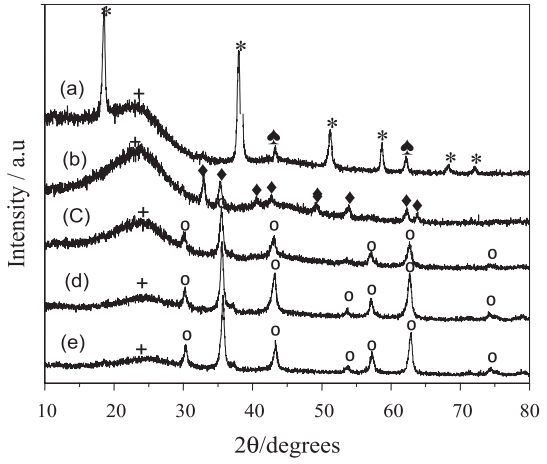

Figure 2. X-ray diffratograms for the (a) AC sample (activated carbon), and for the (b) 2.5IAC, (c) 5IAC (d) 10IAC and (e) 15IAC samples (activated carbon-supported iron oxide). The numbers represent the iron amount (wt.%) in the solids. (♠): magnesium oxide (MgO); (*) magnesium carbide (Mg_2C_3); (+) activated carbon; (0) magnetite (Fe_3O_4); (◆) hematite (Fe_2O_3).

of hematite (JCPDS card 87-1166). The particle sizes of magnetite and hematite calculated by Scherrer equation are shown in Table 2. As expected, the size increased with the iron amount in the catalysts.

Mössbauer spectroscopy

The Mössbauer spectra of the samples are shown in Figure 3 and the hyperfine parameters are displayed in

Table 2. Particle sizes of magnetite and hematite calculated from the X-ray diffractograms for the 2.5IAC, 5IAC, 10IAC and 15MAC samples (activated carbon-supported iron oxide). The numbers represent the iron amount (wt.%) in the solids

Sample	2.5IAC	5IAC	10 IAC	15IAC
Particle size / nm	23	28	32	34

Table 3. Except for the iron poor sample (2.5IAC), all spectra showed a central doublet with shoulders on both sides and two wide lines in the range of negative and positive velocities. In addition, the valleys between these peaks do not reach the baseline and because of this the background seems curved. This is a characteristic of systems with magnetic relaxation due to the small crystal sizes. All spectra were fitted with two magnetically blocked sextuplets, two relaxing sextuplets and a doublet.

The two magnetically blocked and partially resolved sextuplets (blue curves in Figures 3a-3c) can be assigned

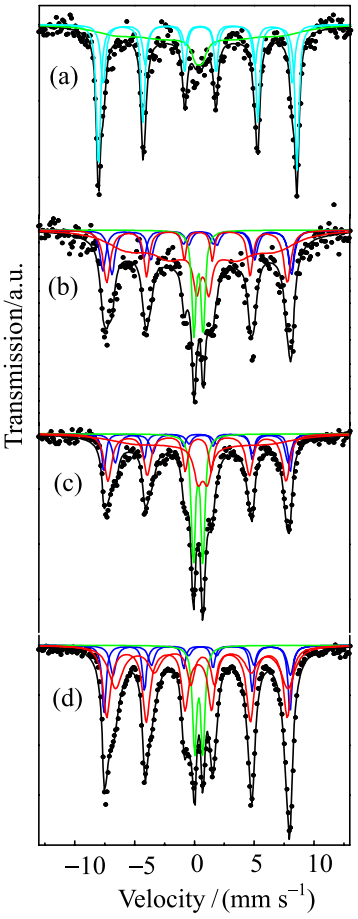

Figure 3. Mössbauer spectra for the (a) 2.5 IAC, (b) 5IAC, (c) 10IAC and (d) 15IAC samples (activated carbon-supported iron oxide). The numbers represent the iron amount (wt.%) in the solids. The blues lines represent magnetically blocked magnetite or hematite, the red one the relaxing magnetite or hematite and the green ones represent supermagnetic hematite.

to the Fe^{3+} ions located in tetrahedral sites (A sites) and to the $Fe^{2.5+}$ ions in the octahedral sites (B sites) of magnetite (Fe_3O_4).[36] The values of hyperfine magnetic fields are slightly decreased compared to typical values of bulk magnetite. This can be attributed to the existence of "collective magnetic excitations" due to the small size of the crystals.[37]

The two relaxing sextuplets (red curves in Figures 3a-3c) were fitted using the model of two-state relaxation proposed by Blume and Tjon[38] and also have typical hyperfine parameters of the A and B sites of magnetite, but now, the hyperfine magnetic fields are even smaller than those magnetically blocked due to magnetic relaxation effects.[39]

These results indicate a broad distribution of magnetite particle sizes, so that the fraction related to the larger particle sizes produces magnetically blocked signals but with reduced fields due to fluctuations of the magnetization vector around the easy magnetization directions, while the fraction of smaller particle sizes produces magnetically relaxing signals. Also, when magnetite particles have sizes small enough to show superparamagnetic relaxation and the signal collapses to a singlet,[39,40] it is reasonable to rule out that the central doublet (green line in Figure 3) corresponds to this species. Besides, it does not seem probable that this doublet, with a typical isomer shift of Fe^{3+}, may correspond to paramagnetic Fe^{3+} ions exchanged or widespread within the activated carbon, since these kinds of supports do not exhibit these characteristics. For these reasons, the doublet is assigned to superparamagnetic hematite (α-Fe_2O_3).

From the Mössbauer results, it is possible to propose a route of formation of magnetite particles on activated carbons as illustrated in Figure 4. It is supposed that the magnetite particles are formed mainly inside the support pores, during heating, from impregnated iron nitrate. It is believed that hematite is produced first since there is no Fe^{2+} species from the starting materials. After some time, carbon monoxide is produced from activated carbon and is able to reduce some Fe^{3+} to Fe^{2+} species to produce magnetite. However, as the reduction should begin on the surface, it is probable that some hematite remains as a core in the particle because of the inaccessibility of carbon monoxide. Therefore, the resulting particles are made of a hematite core surrounded by magnetite.

The iron poor solid (2.5IAC) showed a different spectrum as compared to the other samples. Only hematite could be identified in three different magnetic regimes: magnetically locked, in collective magnetic excitation and in magnetic relaxation state. The first fraction corresponds to the larger particles while the second one has a size large enough to show a not relaxing behavior but their magnetic hyperfine field was decreased by the collective magnetic excitation phenomena.[37] Finally, the third corresponds

Table 3. Hyperfine parameters for the 2.5IAC, 5IAC, 10IAC and 15IAC samples (activated carbon-supported iron oxide). The numbers represent the iron amount (wt.%) in the solids

Species	Parameter	2.5 IAC	5IAC	10% Fe/C	15% Fe/C
Fe^{3+} in A sites of Fe_3O_4	H / T	–	48.9 ± 0.9	48.3 ± 0.2	48.22 ± 0.08
	δ / (mm s^{-1})	–	0.28[a]	0.28[a]	0.28[a]
	2ε / (mm s^{-1})	–	–0.11[a]	–0.11[a]	–0.11[a]
	%	–	13 ± 5	11 ± 3	13 ± 2
$Fe^{"2.5"+}$ in B sites of Fe_3O_4	H / T	–	46.6 ± 0.5	44.8 ± 0.3	46.0[a]
	δ / (mm s^{-1})	–	0.66[a]	0.66[a]	0.66[a]
	2ε / (mm s^{-1})	–	–0.09[a]	–0.09[a]	–0.09[a]
	%	–	14 ± 3	12 ± 2	9 ± 2
Fe^{3+} in A sites of relaxing Fe_3O_4	H / T	–	48.0[a]	46.5 ± 0.4	46.9 ± 0.2
	δ / (mm s^{-1})	–	0.28[a]	0.28[a]	0.28[a]
	2ε / (mm s^{-1})	–	–0.11[a]	–0.11[a]	–0.11[a]
	%	–	19 ± 6	29 ± 4	39 ± 2
$Fe^{"2.5"+}$ in B sites of relaxing Fe_3O_4	H / T	–	45.1[a]	44.7[a]	45.7 ± 3
	δ / (mm s^{-1})	–	0.66[a]	0.66[a]	0.66[a]
	2ε / (mm s^{-1})	–	–0.09[a]	–0.09[a]	–0.09[a]
	%	–	43 ± 6	31 ± 3	29 ± 3
α-Fe_2O_3	H / T	51.5 ± 0.1	–	–	–
	δ / (mm s^{-1})	0.37 ± 0.02	–	–	–
	2ε / (mm s^{-1})	–0.22 ± 0.03	–	–	–
	%	42 ± 4	–	–	–
α-Fe_2O_3 with collective magnetic excitations	H / T	50.7 ± 0.4	–	–	–
	δ / (mm s^{-1})	0.36 ± 0.04	–	–	–
	2ε / (mm s^{-1})	–0.19 ± 0.08	–	–	–
	%	36 ± 8	–	–	–
Relaxing α-Fe_2O_3	H (T)	48.0[a]	–	–	–
	δ / (mm s^{-1})	0.37[a]	–	–	–
	2ε / (mm s^{-1})	0[a]	–	–	–
	%	22 ± 5	–	–	–
α-Fe_2O_3 (sp)	δ / (mm s^{-1})	–	0.77 ± 0.05	0.80 ± 0.02	0.69 ± 0.01
	2ε / (mm s^{-1})	–	0.35 ± 0.03	0.32 ± 0.01	0.37 ± 0.01
	%	–	11 ± 1	17 ± 1	10 ± 1

H: magnetic hyperfine field; δ: isomer shift, 2ε: quadrupole shift; Δ: quadrupole splitting, [a]parameter set during the adjustment. Site A: Fe_3O_4 tetrahedral sites; site B: Fe_3O_4 octahedral sites

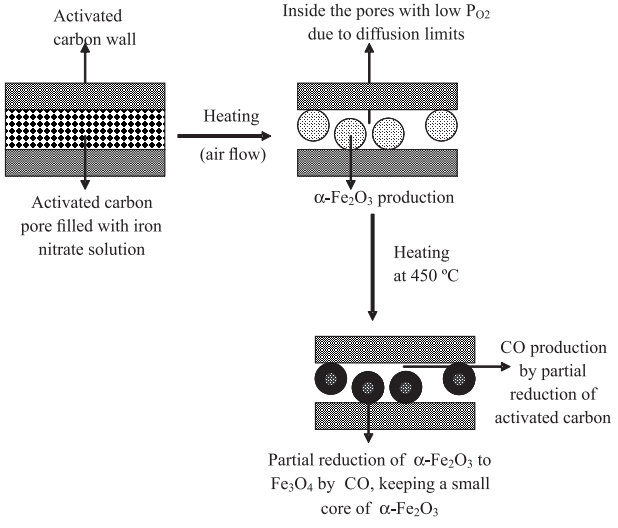

Figure 4. Scheme showing the production of magnetite particles inside the pores of the activated carbon keeping core of hematite.

to very small particles which are in a state of magnetic relaxation. Considering the previous description related to the richest iron catalysts, one can suppose that as the iron load gets very low, the occlusion of carbon pores is negligible. Therefore, diffusion restrictions for the iron richest samples are also negligible. As a result, the carbon monoxide formed by the partial combustion of the support is rapidly eliminated, so that the partial reduction of hematite to magnetite does not occur.

Table 4 shows the total percentages of both magnetite and hematite for the samples, except for the iron poor solid. It can be noted that magnetite is the major component and that no significant difference between the percentages of the phases for the different catalysts within experimental error. These results are consistent with the fact that the three samples show strong magnetic response under an external magnetic field.

Table 4. Amounts of magnetite (Fe_3O_4) and of supermagnetic hematite (α-Fe_2O_3 (sp)) in the catalysts obtained from Mössbauer spectra of 5IAC, 10IAC and 15IAC samples (activated carbon-supported magnetite). The numbers represent the iron amount (wt.%) in the solids

Sample	Amount of the species	
	Fe_3O_4 / %	α-Fe_2O_3 (sp) / %
5IAC	89 ± 19	11 ± 1
10IAC	83 ± 12	17 ± 1
15IAC	90 ± 8	10 ± 1

It was not possible to calculate the particle sizes from the Mössbauer spectra since there are magnetic relaxation effects. Therefore, the percentage in which hyperfine magnetic fields are decreased by the relaxation and by effects of collective magnetic excitations cannot be known. However, it is possible to conclude that the particle sizes increase in the order 2.5IAC < 5IAC < 10IAC < 15IAC, just as the magnetic blockage does.

Specific surface area and porosity measurements

All samples show type II isotherms typical of micro and mesoporous materials, with a hysteresis loop, indicating the capillary condensation in mesopores, as shown in Figure 5. Table 5 displays the main textural properties of the samples. As can be seen, the impregnation of activated carbon with

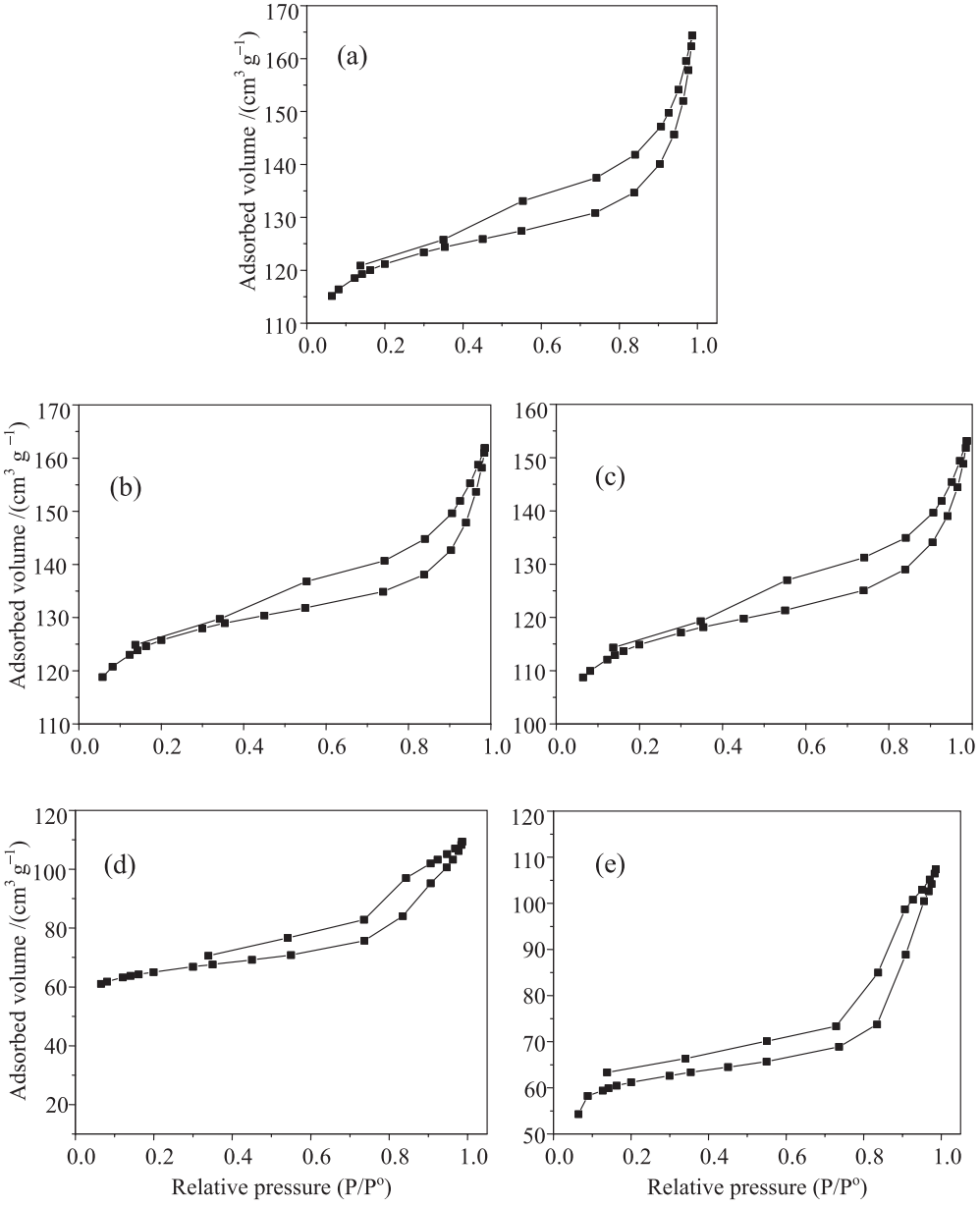

Figure 5. Adsorption and desorption isotherms for the (a) AC sample (activated carbon), and for the (b) 2.5IAC, (c) 5IAC, (d) 10IAC and (e) 15IAC sample (activated carbon-supported iron oxide). The numbers represent the iron amount (wt.%) in the solids.

Table 5. Textural properties of the AC sample (activated carbon), and for the 2.5 MAC, 5MAC, 10MAC and 15MAC samples (activated carbon-supported iron oxide). The numbers represent the iron amount (wt.%) in the solids

Sample	S_{BET} / (m^2 g^{-1})	Micropore area, *t*-plot / (m^2 g^{-1})	Pore volume, BJH / (cm^3 g^{-1})	Micropore volume / (cm^3 g^{-1})	Mesopore volume / (cm^3 g^{-1})
AC	408	320	0.24	0.149	0.087
2.5IAC	426	333	0.25	0.154	0.076
5IAC	388	297	0.23	0.138	0,079
10IAC	220	160	0.16	0.074	0.085
15IAC	210	151	0.16	0.069	0.086

S_{BET}: specific surface area by BET method.

small iron amounts (2.5 and 5%) does not affect its textural properties. This finding indicating that the occlusion of the pores of the carbon support is negligible, in agreement with the Mössbauer results. However, higher amounts of iron (10 and 15%) caused a large decrease in the specific surface areas, which is closely related to the decrease in micropore area and volume. This confirms the supposition that most of iron oxide is deposited inside the pores, where it partially blocks the pores.

Temperature programmed reduction

Figure 6 shows the reduction profiles of the catalysts. For the 5IAC sample, it can be seen a large peak centered at 599 °C, assigned to hematite and magnetite reduction to produce magnetite and metallic iron, respectively, as previously found.[41,42] The increase of iron amount shifted this peak to higher temperatures as shown by the curves of the other samples. A small and broad peak around 400 °C can be related to the reduction of hematite on the surface.[41] A large negative peak at high temperatures can be assigned to the decomposition of the functional groups on the activated carbon surface.

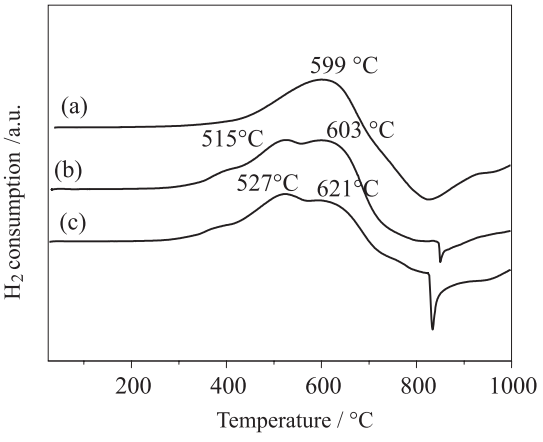

Figure 6. Curves of temperature programmed reduction for the (a) 5IAC, (b) 10IAC and (c) 15IAC samples (activated carbon-supported magnetite). The numbers represent the iron amount (wt.%) in the solids.

Methylene blue removal on the catalysts

Figure 7 shows the methylene blue removal as a function of time during Fenton reaction. It can be noted that methylene blue removal increased with iron amount in the solids. This could be related to the increase of the amount of active sites available to reaction. Therefore, the iron rich sample (15IAC) is the most active catalyst while the iron poor solid (2.5IAC) is the least active one. However, the activated carbon itself is also able to remove methylene blue, in fact it removed more dye than the iron poor sample (2.5IAC). As activated carbon is not active in Fenton reaction, a significant contribution of methylene blue adsorption for the dye removal should be expected. This contribution was confirmed by the experiments carried out in the absence of hydrogen peroxide, as shown in Figure 8. Both activated carbon and the catalysts are able to adsorb methylene blue in a large extension and then the adsorption is the dominant process in the dye removal. This process increased rapidly with time suggesting that it is faster than Fenton reaction. However, there is not a simple relationship between the adsorption capacity and the textural properties of the samples, a fact that can be related to the chemical nature of the adsorption as well as to the chemical surface of activated carbons.[8] Therefore, this capacity is much more related to the kind and amount of the functional groups on the surface of activated carbon in each sample. As can be seen, the activated carbon and the iron poor samples (2.5 and 5%) showed similar specific surface areas and similar adsorption capacity and the same behavior was noted for the iron rich ones (10 and 15%). On the other hand, the first samples showed higher specific surface areas (388-426 m^2 g^{-1}) but lower adsorption capacity than the other ones which showed lower specific surface areas (210-220 m^2 g^{-1}). These findings suggest that low amounts of iron do not change significantly the sites of adsorption for methylene blue, as compared to activated carbon, while higher amounts lead to the production of different species creating new sites for adsorption. It

seems that the production of these new sites is not related to specific surface areas.

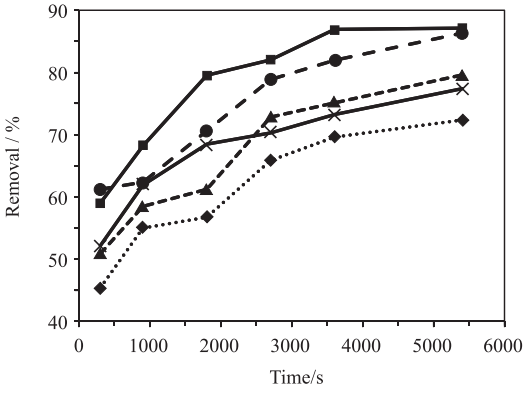

Figure 7. Methylene blue removal over the catalysts as a function of time during the Fenton reaction: AC sample (×) (activated carbon), and 2.5IAC (◆), 5IAC (▲) 10IAC (●) and 15IAC (■) samples (activated carbon-supported iron oxide). The numbers represent the iron amount (wt.%) in the solids.

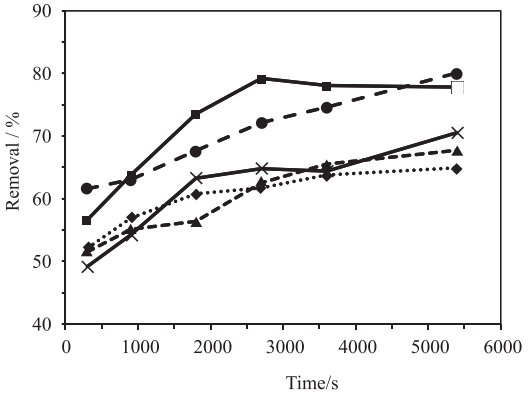

Figure 8. Methylene blue removal by adsorption on the catalysts as a function of time during the Fenton reaction, AC sample (×) (activated carbon), and 2.5IAC (◆), 5IAC (▲), 10IAC (●) and 15IAC (■) samples (activated carbon-supported iron oxide). The numbers represent the iron amount (wt.%) in the solids.

As the activity of magnetite in the Fenton reaction, as well as the activity of hydroxyl ions to oxidize the methylene blue, are well known,[15,20] one can suppose that both adsorption and reaction occurs simultaneously, as shown in Figure 9. It is expected that hydroxyl groups can react with the methylene blue adsorbed or in solution. From Figures 7 and 8, we can to conclude that the adsorption process is faster and then dominant in the dye removal.

Table 6 shows the percentages of methylene blue removed from the effluent, obtained by the difference between the data in Figures 7 and 8. This difference should reflect the activity of the catalysts in Fenton reaction. However, there is an increase of the dye removal by activated carbon itself which cannot be assigned to Fenton reaction. In this case, the hydrogen peroxide is probably creating new surface groups on activated carbons[8] able to adsorb methylene blue. Except

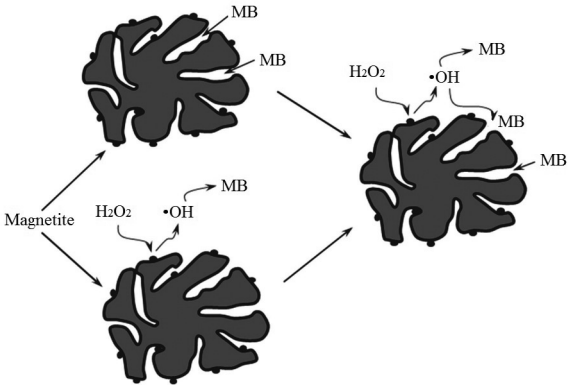

Figure 9. Scheme showing the adsorption and/or oxidation of methylene blue (MB) with hydroxyl radicals on activated carbon-supported magnetite.

for the 15IAC sample, all iron-containing solids showed less adsorption capacity in the presence of hydrogen peroxide in the beginning of the process. This indicates that the Fenton reaction is not occurring and probably iron affects the types of the surface groups on the activated carbon surface, as previously found for magnesium and vanadium.[8] Therefore, due to the high adsorption capacity of activated carbon as well as the effect of metals and hydrogen peroxide on its surface composition,[8] it is not possible to state the fraction of methylene blue removal related only to adsorption or only to Fenton reaction. From Table 6, it can be noted that there is not a single relationship between the methylene blue removal and iron concentration. This fact can be explained by the different iron species produced in the solids, as detected by Mössbauer spectroscopy, as well as by the ability of these species in affecting the types of functional groups on the surface of activated carbon, which promotes methylene blue adsorption. These findings are in agreement with previous work,[13] according to which activated carbon/iron oxide composites showed high efficiency to remove methylene blue from solution by combined adsorption and oxidation process.

Table 6. Methylene blue removal calculated from Figures 7 and 8 for the AC sample (activated carbon), and for the 2.5 MAC, 5MAC, 10MAC and 15MAC samples (activated carbon-supported iron oxide). The numbers represent the iron amount (wt.%) in the solids

time / s	Methylene blue removed by Fenton reaction / %				
	AC	2.5IAC	5IAC	10IAC	15IAC
300	3.07	–6.70	–0.57	–0.36	2.36
900	7.62	–1.90	3.36	–0.69	4.39
1800	5.20	–4.09	4.85	2.96	6.01
2700	5.51	4.12	10.28	6.72	2.81
3600	8.86	5.80	9.59	7.33	8.86
5400	6.89	7.40	11.91	6.25	9.35

Conclusions

Samples of activated carbon-supported magnetite with different iron amounts (2.5, 5, 10 and 15%) were successfully prepared from coconut shells, offering a possibility of reducing the agricultural wastes in the environment. The solids show different textural and reducing properties depending on the presence and on the amount of iron. Except for the iron poor sample (2.5%) which was made of hematite, the magnetite particles were found to have a core of hematite and their sizes (28-34 nm) increase with iron amount in solids. These solids were able to remove up to 88% of methylene blue from aqueous solutions, mainly by dye adsorption which was supposed to be faster than Fenton reaction. The solid with 15% of iron was the most active one, a fact that can be related the highest amount of iron on the surface promoting Fenton reaction and creating new functional groups on the surface of activated carbon, able to adsorb methylene blue. The preparation and use of these catalysts can contribute to overcome two problems faced nowadays: the decrease of organic wastes in the environment and the purification of textile effluents preserving the water resources.

Acknowledgements

S. B. L. and S. M. S. B. acknowledge Conselho Nacional de Desenvolvimento Científico e Tecnológico (CNPq) for their graduate fellowships. The authors are grateful to CNPq and Petrobras S.A.

References

1. Gonzalez, M. P. E.; Montoya, V. H.; *Bioresour. Technol*. **2009**, *100*, 2111.
2. Nabais, J. M. V.; Laginhas, C. E. C.; Carrott, P. J. M.; Carrott, M. M. L. R.; *Fuel Process. Technol.* **2011**, *92*, 234.
3. Oliveira, S. B.; Rabelo, D.; Rangel, M. C.; *Stud. Surf. Sci. Catal.* **2005**, *156*, 609.
4. Park, S. J.; Jung, W. Y.; *J. Colloid Interface Sci.* **2002**, *250*, 196.
5. Afkhami, A.; Madrakian, T.; Karimi, Z.; Amini, A.; *Colloids Surf., A* **2007**, *304*, 36.
6. Thomas, K. M.; *Catal. Today* **2007**, *120*, 389.
7. Rangel, M. C.; Oliveira, S. B.; Barbosa, D. P.; Monteiro, A. P. M.; Rabelo, D.; *Catal. Today* **2008**, *133-35*, 92.
8. Holtz, R. D.; Oliveira, S. B.; Fraga, M. A.; Rangel, M. C.; *Appl. Catal., A* **2008**, *350*, 79.
9. Rangel, M. C.; Britto, J. M.; Oliveira, S. B.; Rabelo, D.; *Catal. Today* **2008**, *133-35*, 582.
10. Barbosa, D. P.; Tchiéta, P.; Rangel, M. C.; Epron, F.; *J. Mol. Catal.* **2013**, *366*, 294.
11. Stavropoulos, G. G.; Samaras, P.; Sakellaropoulos, G. P.; *J. Hazard. Mater.* **2008**, *151*, 414.
12. Chen, Y; Zhu, Y.; Wang, Z.; Li, Y; Wang, L.; Ding, L.; Gao, X.; Ma, Y.; GA, Y.; *Adv. Colloid Interface Sci.* **2011**, *163*, 39.
13. Castro, C. S.; Guerreiro, M. C.; Oliveira, L. C. A.; Gonçalves, M.; *Quim. Nova* **2009**, *32*, 1561.
14. Pielesz, A.; *J. Mol. Struct.* **1999**, *512*, 337.
15. Pérez, M.; Torrades, F.; Doménech, X.; Peral, J.; *Water Res.* **2002**, *36*, 2703.
16. Britto, J. M.; Rangel, M. C.; *Quim. Nova* **2008**, *31*, 114.
17. Pignatello, J. J.; Oliveros, E.; Mackay, A.; *Crit. Rev. Env. Sci. Technol.* **2006**, *36*, 1.
18. Cuzzola, A.; Bernini, M.; Salvadori, P. A.; *Appl. Catal., B* **2002**, *36*, 231.
19. Xue, X.; Hanna, K.; Despas, C.; Wu, F.; Deng, N.; *J. Mol. Catal. A:Chem.* **2009**, *311*, 29.
20 . Miller, C. M.; Valentine, R. L.; *Water Res.* **1999**, *33*, 2805.
21. Huang, H. H.; Lu, M. C.; Chen, J. N.; *Water Res.* **2001**, *35*, 2291.
22. Matta, R.; Hanna, K.; Chiron, S.; *Sci. Total Environ.* **2007**, *385*, 242.
23. Bruce, I. J.; Taylor, J.; Todd, M.; Davies, M. J.; Borioni, E.; Sangregorio, C.; Sem, T.; *J. Magn. Magn. Mater.* **2004**, *284*, 145.
24. Arruebo, M.; Fernandez-Pacheco, R.; Irusta, S.; Arbiol, J.; Ibarra, M. R.; Santamaria, J.; *Nanotechnology* **2006**, *17*, 4057.
25. Yuan, P.; Fan, M.; Yang, D.; He, H.; Liu, D.; Yuan, A.; Zhu, J. X.; Chen, T.; *J. Hazard Mater.* **2009**, *166*, 821.
26. Oliveira, L. C. A.; Rios, R. V. R. A.; Fabris, J. D.; Gargc, V.; Sapag, K.; Lago, R. M.; *Carbon* **2002**, *40*, 2177.
27. Pereira, M. C.; Coelho, F. S.; Nascentes, C. C.; Fabris, J. D.; Araújo, M. H.; Sapag, K.; Oliveira, L. C. A.; Lago, R. M., *Chemosphere* **2010**, *81*, 7.
28. Boonamnuayvitaya, V.; Sae-Ung, V.; Tanthapanichakoon, S.; *Sep. Purif.* **2005**, *42*, 159.
29. Puziy, A. M.; Poddubnaya, O. I.; Martínez-Alonso, A.; Castro-Muniz, A.; Suárez-García, F.; Tascón, J. N. D.; *Carbon* **2007**, *45*, 1941.
30. Yang, T.; Lua, A. C.; *J. Colloid Interface Sci.* **2003**, *267*, 408.
31. Rockstraw, D. A.; *Microporous Mesoporous Mater.* **2007**, *100*, 12.
32. Jozwiak, W. K; Kaczmarek, E.; Maniecki, T. P.; Ignaczak, W.; Maniukiewicz, W.; *Appl. Catal., A* **2007**, *326*, 17.
33. Oya, A.; Marsh, H.; *J. Mater. Sci.* **1982**, *17*, 309.
34. Cotton, F. A.; Wilkinson, G.; *Advanced Inorganic Chemistry*, 5th ed.; Wiley: New York, USA, 1988.
35. Wang, K.; Li, W. S.; Zhou, X. P.; *J. Mol. Catal. A: Chem*. **2008**, *283*, 153.
36. Vandenberghe, R. E.; De Grave, E.; Landuydt, C.; Bowen, L. H.; *Hyperfine Interact.* **1990**, *53*, 175.
37. Mørup, S.; Topsøe, H.; *Appl. Phys.* **1976**, *11*, 63.

38. Blume, M.; Tjon, J. A.; *Phys. Rev.* **1968**, *165*, 446.
39. Rancourt, D. G.; Daniels, J. M.; *Phys. Rev*. **1984**, *29*, 2410.
40. van Lierop, J.; Ryan, D. H.; *Phys. Rev. B: Condens. Matter Mater. Phys.* **2001**, *63*, 0644061-8.
41. de Araujo, G. C.; Rangel, M. C.; *Catal. Today* **1999**, *62*, 201.
42. Pereira, A. L. C.; Berrocal, G. J. P.; Marchetti, S. G.; Albornoz, A.; de Souza, A. O.; Rangel, M. C.; *J. Mol. Catal. A: Chem.* **2008**, *281*, 66.

Submitted: October 5, 2012
Published online: February 28, 2013

FAPESP has sponsored the publication of this article.